Structure

Article

# Cryo-EM structure of a monomeric RC-LH1-PufX supercomplex with high-carotenoid content from *Rhodobacter capsulatus*

## Graphical abstract

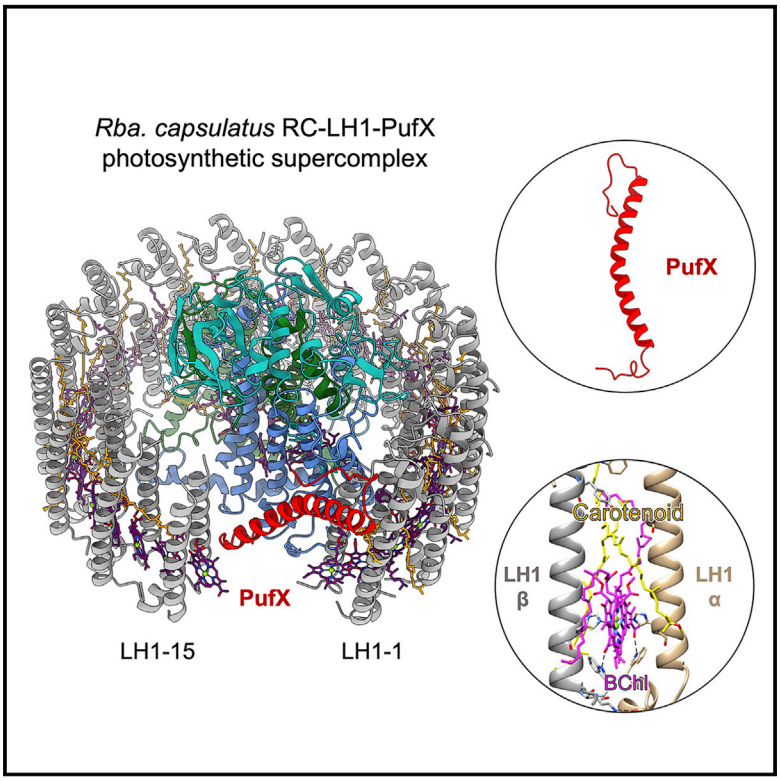


## Highlights

- The photosynthetic RC-LH1 core complex of *Rhodobacter capsulatus* forms a monomer
- The LH1 ring surrounding RC contains 15 LH1 subunits and PufX, mediating an opening
- Each LH1 αβ subunit contains two BChls and two carotenoids
- Structural flexibility of the last LH1 subunits results in varying degrees of opening

## Authors

Laura Bracun, Atsushi Yamagata, Bern M. Christianson, Mikako Shirouzu, Lu-Ning Liu

## Correspondence

luning.liu@liverpool.ac.uk

## In brief

Bracun et al. report the cryo-EM structure of the reaction center-light-harvesting-1-PufX supercomplex, a key photosynthetic complex in the phototropic purple bacterium *R. capsulatus*. The detailed structural analysis provides insights into light harvesting, electron transport, and the structural diversity of the photosynthetic core complexes from various bacterial species.

Bracun et al., 2023, Structure *31*, 1–11
March 2, 2023 
https://doi.org/10.1016/j.str.2023.01.006

CellPress

Please cite this article in press as: Bracun et al., Cryo-EM structure of a monomeric RC-LH1-PufX supercomplex with high-carotenoid content from *Rhodobacter capsulatus*, Structure (2023), https://doi.org/10.1016/j.str.2023.01.006

Structure

CellPress
OPEN ACCESS

Article

# Cryo-EM structure of a monomeric RC-LH1-PufX supercomplex with high-carotenoid content from *Rhodobacter capsulatus*

Laura Bracun,[1,2] Atsushi Yamagata,[2] Bern M. Christianson,[1] Mikako Shirouzu,[2] and Lu-Ning Liu[1,3,4,*]
[1]Institute of Systems, Molecular and Integrative Biology, University of Liverpool, Liverpool L69 7ZB, UK
[2]Laboratory for Protein Functional and Structural Biology, RIKEN Center for Biosystems Dynamics Research, 1-7-22 Suehiro-cho, Tsurumi-ku, Yokohama, Kanagawa 230-0045, Japan
[3]College of Marine Life Sciences and Frontiers Science Center for Deep Ocean Multispheres and Earth System, Ocean University of China, Qingdao 266003, China
[4]Lead contact
*Correspondence: luning.liu@liverpool.ac.uk
https://doi.org/10.1016/j.str.2023.01.006

## SUMMARY

In purple photosynthetic bacteria, the photochemical reaction center (RC) and light-harvesting complex 1 (LH1) assemble to form monomeric or dimeric RC-LH1 membrane complexes, essential for bacterial photosynthesis. Here, we report a 2.59-Å resolution cryoelectron microscopy (cryo-EM) structure of the RC-LH1 supercomplex from *Rhodobacter capsulatus*. We show that *Rba. capsulatus* RC-LH1 complexes are exclusively monomers in which the RC is surrounded by a 15-subunit LH1 ring. Incorporation of a transmembrane polypeptide PufX leads to a large opening within the LH1 ring. Each LH1 subunit associates two carotenoids and two bacteriochlorophylls, which is similar to *Rba. sphaeroides* RC-LH1 but more than one carotenoid per LH1 in *Rba. veldkampii* RC-LH1 monomer. Collectively, the unique *Rba. capsulatus* RC-LH1-PufX represents an intermediate structure between *Rba. sphaeroides* and *Rba. veldkampii* RC-LH1-PufX. Comparison of PufX from the three *Rhodobacter* species indicates the important residues involved in dimerization of RC-LH1.

## INTRODUCTION

Photosynthetic reaction centers (RCs) are integral membrane pigment-protein complexes, which catalyze light-driven electron transport and energy conversion. In purple phototrophic bacteria, the RC and light-harvesting complex 1 (LH1) form an RC-LH1 core supercomplex, essential for the primary reactions of photosynthesis.[1–3] The RC-LH1 core complexes collect photons directly from sunlight or the peripheral antenna, LH2, and then perform charge separation to generate electrons, reduce quinone to quinol, and oxidize C-type cytochrome (Cyt) proteins.[4,5] The RC-LH1 architecture ensures the shuttling of electrons between the RC and the Cyt $bc_1$ complex. This cyclic electron flow results in an electrochemical gradient across the photosynthetic membrane, generating a proton motive force (pmf) to ultimately power ATP production.[5,6]

Although the RC-LH1 core complexes fulfill the same function in different phototrophic prokaryotes, their native architectures exhibit large variations.[7] Some species adopt a monomeric RC-LH1 structure in which the central RC is encircled by a closed near-circular array of 16 LH1 αβ-heterodimers[8–13] or double LH1 rings (16 LH1 subunits in the inner ring and 24 LH1 subunits in the outer ring).[14] In contrast, some species develop an open LH1 array with a gap or gaps to form the RC-LH1 monomer or dimer.[11,15–23] All members of the genus *Rhodobacter* incorporate a transmembrane polypeptide PufX in their RC-LH1 complexes, resulting in an open LH1 architecture. Recent cryoelectron microscopy (cryo-EM) studies have deciphered the structural details of the RC-LH1-PufX dimer structure of *Rhodobacter* (*Rba.*) *sphaeroides*[18,24,25] and the RC-LH1-PufX monomer structure of *Rba. veldkampii*.[19] Despite these structural analyses and previous studies,[22,26–28] the mechanism underlying the RC-LH1 dimerization mediated by PufX remains still obscure.

*Rba. capsulatus* has been widely used as a model organism to study bacterial photosynthesis and develop biotechnological applications.[29–31] To date, there is no structure reported for the *Rba. capsulatus* RC-LH1 core complex. Here, we report the cryo-EM structure of the monomeric RC-LH1 supercomplex from *Rba. capsulatus* at 2.59-Å resolution. The structure shows that the *Rba. capsulatus* RC-LH1 complex forms exclusively a monomer in which the RC is surrounded by 15 LH1 subunits; incorporation of PufX features a large PufX-mediated gap within the LH1 ring, which may function as a dedicated quinone channel. Each LH1 subunit contains two bacteriochlorophylls (BChls) and two carotenoids, forming an intense pigment network. The unique architecture ensures efficient light harvesting and photoprotection as well as quinone/quinol exchange predominantly through the PufX-mediated gap within LH1. Our study provides

Please cite this article in press as: Bracun et al., Cryo-EM structure of a monomeric RC-LH1-PufX supercomplex with high-carotenoid content from *Rhodobacter capsulatus*, Structure (2023), https://doi.org/10.1016/j.str.2023.01.006



insights into the general assembly principles, structural flexibility, and diversity of PufX-containing photosynthetic RC-LH1 core complex structures from distinct *Rhodobacter* species.

## RESULTS AND DISCUSSION

### Overall RC-LH1 architecture

The photosynthetic RC-LH1 core complexes are located in the vesicular intracytoplasmic membranes (namely chromatophores) in *Rba. capsulatus* cells, which have an average diameter of 57 ± 11 nm (n = 100) (Figure S1A), which is in good agreement with previous studies[32] and is comparable to those in *Rba. sphaeroides* (50–60 nm)[33–37] and *Rba. veldkampii* (~50 nm).[38] Following the same isolation procedure that was applied in obtaining native RC-LH1 monomers from *Rba. veldkampii*[38] and both RC-LH1 monomers and dimers from *Rba. sphaeroides*,[18] we purified the native RC-LH1 core complex from photoheterotrophically grown wild-type (WT) *Rba. capsulatus* cells, and they form exclusively monomers (Figures S1B, S2A, and S2B), consistent with previous findings.[22] This indicates that dimerization of RC-LH1 is not essential for the curvature of chromatophore membranes, corroborating the finding in *Rba. veldkampii*.[38]

The isolated RC-LH1 complexes were subjected to cryo-EM single-particle analysis (Figure S2). From a total of 935,709 particles, 181,054 particles that could be categorized into well-defined classes were used for final 3D reconstruction. Cryo-EM analysis determined the structure of the *Rba. capsulatus* RC-LH1 core complex at 2.59-Å resolution (Figure S2; Table S1). An atomic model was built based on the experimentally obtained map (Figures 1, S3, and S4).

The *Rba. capsulatus* RC-LH1 core complex is made of a central three-subunit RC (RC-L, RC-M, RC-H) surrounded by an open, near-circular ring of 15 LH1 αβ heterodimers with the dimensions 120 × 112 × 75 Å (Figure 1A). The LH1 array is interrupted by a transmembrane PufX polypeptide (Figure 1B), which is in a position equivalent to that of PufX in *Rba. veldkampii*[19] and *Rba. sphaeroides*.[18,20,21] The cryo-EM structure reveals that this RC-LH1-PufX core complex contains 30 BChls *a* and 28 carotenoid pigments in the LH1 ring, consistent with the reported light-harvesting peptide:carotenoid:BChl *a* ratio of 1:1:1 in previous studies.[39,40] Each LH1 αβ heterodimer contains two BChls *a* and two carotenoids (rather than one carotenoid identified in its counterpart in *Rba. veldkampii*[19]). The RC binds four BChls *a* (two of which make up the special pair), two bacteriopheophytins (BPheos), two ubiquinones (primary quinone $Q_A$ and secondary quinone $Q_B$), a non-heme iron, and a carotenoid. Moreover, two additional quinones were identified in positions near the $Q_B$ site equivalent to those in other RC-LH1 complexes (Figure S3).[9,11,19] Seven lipid molecules were identified in the RC-LH1-PufX complex and were assigned as phosphatidylethanolamine (Figure S3) due to its high abundance in *Rba. capsulatus* membranes[41] and the small size of its head group that overall fits better with the cryo-EM densities than the other characterized abundant lipid phosphatidylglycerol (Figure S4).

### The RC structure

The *Rba. capsulatus* RC is composed of RC-L, RC-M, and RC-H subunits, which are largely comparable to those of other purple photosynthetic bacteria reported (Figure S5). The RC-L and RC-M subunits host and position all cofactors important for effective charge separation and electron transport. The periplasmic sides of RC-L and RC-M provide the site for the soluble electron carrier Cyt $c_2$ to bind to the RC.[19,42] The RC-H subunit is located at the cytoplasmic side of the core complex, with a single transmembrane helix anchored into the chromatophore membrane. The RC-H subunit of *Rba. capsulatus* is largely similar in sequence and overall structure to previously reported RC-H subunits of purple photosynthetic bacteria (Figure S6A). However, a marked difference is the presence of a short α-helix above the $Q_A$ site in *Rba. capsulatus* RC-H subunit (Figure S6B), and the sequence region containing the α-helix is highly conserved among some *Rhodobacter* species (Figure S6A). However, this defined secondary structure has not been seen in the same region of any reported RC-LH1 structures, including the *Rba. veldkampii* and *Rba. sphaeroides* counterparts. Interestingly, the RC-H subunit of *Gemmatimonas phototrophica* is fragmented into two peptides in this region.[14] Although the function of this helix remains to be determined, its structural rigidity might be relevant to proton transfer, such as providing enhanced insulation of the $Q_A$ site from the cytoplasm.

### PufX polypeptide

Like all other members of the genus *Rhodobacter*, *Rba. capsulatus* RC-LH1 features an additional polypeptide PufX. The cryo-EM structure reveals that PufX interrupts the LH1 ring and mediates the generation of an opening of 30 Å in distance (Figure 1). This opening prevents the LH1 ring from forming a fully closed architecture and presumably provides the structural basis for efficient quinone exchange between the RC and distant Cyt $bc_1$.[43,44] Consistently, previous studies have shown that the *Rba. capsulatus* cells lost their ability to grow photosynthetically in the absence of PufX under illumination.[45] This is likely ascribed to the fact that higher carotenoid content per LH1 creates more crowded space between LH1 subunits and provides steric hindrance for quinone passage.[46]

The PufX polypeptide spans the membrane diagonally (Figure 2A) and forms interactions with the RC and LH1 subunits mainly through its terminal regions, resembling PufX of *Rba. veldkampii*[19] and *Rba. sphaeroides*.[18,20,21] These terminal regions do not possess ordered secondary structures and are connected by a transmembrane α-helix that makes up the majority of PufX (Figure 2B). The PufX N-terminal region interacts with α-Arg14 and α-Arg15 of the LH1-1 subunit through its Asp5 residue (Figure 2C1; Table S2). In addition, Gln25 of PufX also associates with α-Arg14 of LH1-1. The C-terminal tail of PufX interacts with RC-L: PufX Arg57 and Tyr65 interact with RC-L Asp257 and Ala145, respectively, through hydrogen bonds and salt bridges established by their side chains; Ala61 and Pro64 form hydrogen bonds with RC-L Tyr144 and Asn159, respectively, through their main chain peptide bonds (Figure 2C2; Table S2). At the C-terminal end of the transmembrane α-helix, PufX Ser37 interacts with LH1-15α Met53 (Figure 2C3; Table S2). This interaction may be transient, as the last LH1 subunits have relatively more flexible arrangements. Overall, these interactions play roles in facilitating the anchoring of PufX and the association of the LH1 ring to the RC.

Please cite this article in press as: Bracun et al., Cryo-EM structure of a monomeric RC-LH1-PufX supercomplex with high-carotenoid content from *Rhodobacter capsulatus*, Structure (2023), https://doi.org/10.1016/j.str.2023.01.006



CellPress
OPEN ACCESS

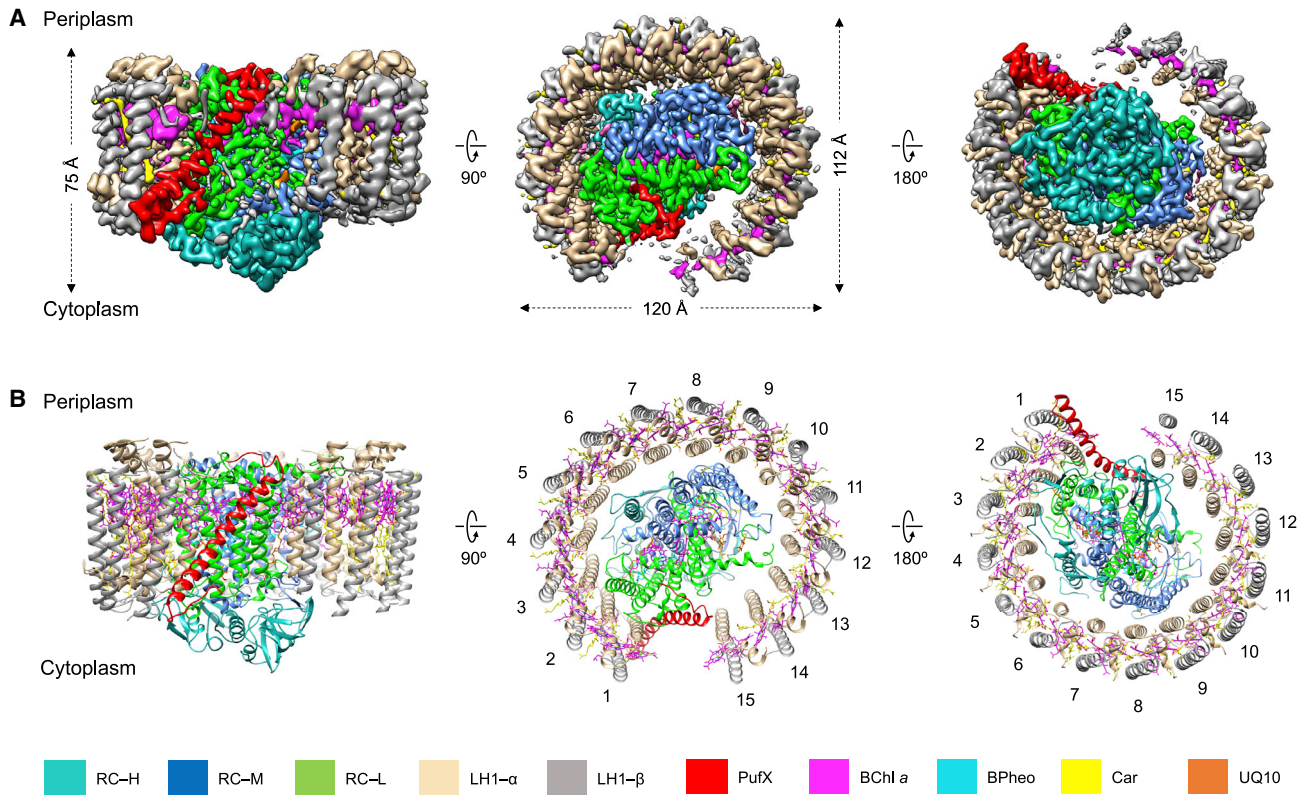


**Figure 1. Overall structure of the RC-LH1-PufX complex from *Rba. capsulatus***

(A) Cryo-EM density map shown in three views from left to right: side view, the view from the periplasmic side of the membrane, and the view from the cytoplasmic side of the membrane. Color scheme is presented at the bottom. Sizes of the complex in x, y, and z directions are noted.

(B) Structural model in orientations respective to (A) and color coded using the same color scheme. The numbers mark each LH1 subunit in the ring.

See also Figures S1–S6 and Table S1.

Although the sequences of PufX polypeptides among *Rhodobacter* species are conserved (Figure S7A), in some *Rhodobacter* species such as *Rba. sphaeroides*, PufX mediates the dimerization of RC-LH1 core complexes,[22,47] and consequently, these species contain both dimeric and monomeric RC-LH1-PufX cores. In contrast, some *Rhodobacter* species, such as *Rba. capsulatus* and *Rba. veldkampii*, possess exclusively RC-LH1-PufX monomers. The overall architectures of *Rba. capsulatus* and *Rba. veldkampii* RC-LH1-PufX monomers are largely similar, while the notable differences between the two RC-LH1-PufX monomers and the *Rba. sphaeroides* RC-LH1-PufX monomer are the number of LH1 subunits, the size of the LH1 opening mediated by PufX, and the presence of PufY (Figure S7). Both *Rba. veldkampii* and *Rba. capsulatus* RC-LH1-PufX form rings of 15 LH1 subunits with an opening of 30 Å; the distance between PufX and the final LH1 subunit at the cytoplasmic side of the membrane is <4 Å (Figure 2C). The *Rba. sphaeroides* RC-LH1-PufX, however, has only 14 LH1 $\alpha\beta$ heterodimers per monomer, resulting in a wider opening (46 Å) within the LH1 ring,[18] which provides enough space for tight association of another RC-LH1-PufX monomer to eventually form the S-shaped dimer. The *Rba. sphaeroides* RC-LH1-PufX possesses another transmembrane polypeptide PufY, also termed protein-Y[21,24] or protein-U,[20,25] which is located between the RC and LH1-13 and LH-14 subunits and prevents LH1-13/14 adjacent to the $Q_B$ site from bending inward toward the RC.[18] In the Δ*pufY Rba. sphaeroides* RC-LH1-PufX complex, the LH1 opening is still larger than those of *Rba. capsulatus* and *Rba. veldkampii* (Figure S7), and the RC-LH1-PufX dimer can still form,[18] which may suggest that the gap size is important for the PufX-mediated dimerization of two RC-LH1 monomers. No PufY homologs were identified in *Rba. capsulatus* and *Rba. veldkampii*, consistent with the cryo-EM structures.

To evaluate how PufX mediates the dimerization of RC-LH1 core complexes, we performed a comparison of the N termini of PufX from *Rba. capsulatus*, *Rba. veldkampii*, and *Rba. sphaeroides*. Note that the PufX C termini are mainly involved in binding with RC-L in the monomer and that their structures were not always fully solved; additionally, we chose the RC-LH1 monomer within the native dimer from *Rba. sphaeroides* instead of the native RC-LH1 monomer for the structural comparison, as their architectures are largely similar and the reported cryo-EM structures of the native *Rba. sphaeroides* RC-LH1 monomer did not offer a sufficient resolution to model the PufX N-terminal region, likely due to its more flexible structure without dimerization.[18,20,21] The analysis reveals that the N-terminal tails of PufX in native monomeric RC-LH1-PufX fold back toward the RC to interact with the LH1-1 subunits, whereas that in the RC-LH1-PufX dimer extends from the RC to associate with the other monomer (Figure 2D). However, these interacting residues

Please cite this article in press as: Bracun et al., Cryo-EM structure of a monomeric RC-LH1-PufX supercomplex with high-carotenoid content from *Rhodobacter capsulatus*, Structure (2023), https://doi.org/10.1016/j.str.2023.01.006



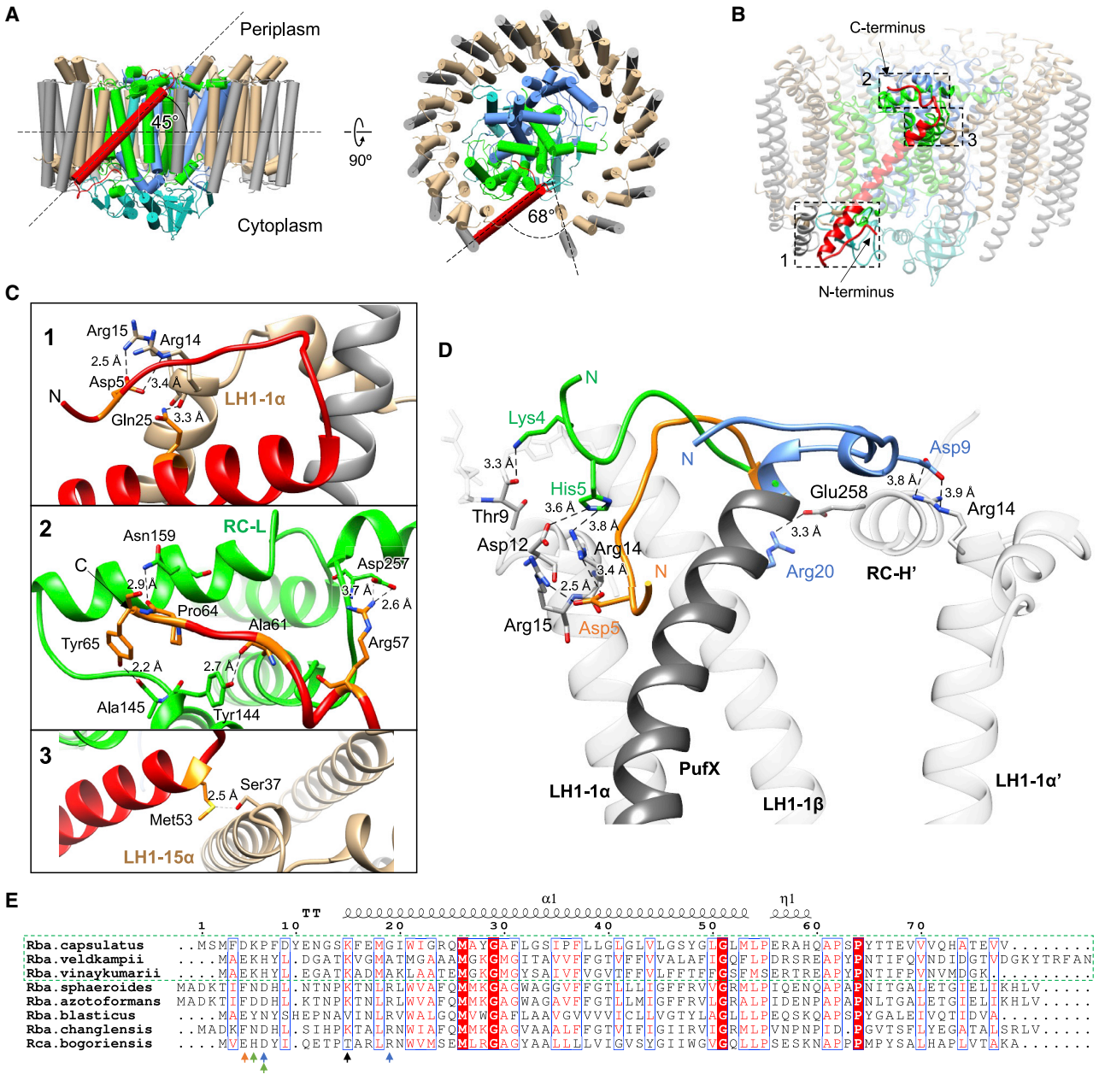


**Figure 2. Position and interactions of PufX in RC-LH1-PufX complex of *Rba. capsulatus***

(A) Structure of the complex with helixes shown as cylinders in the side view (left) and periplasmic view (right). Angles that PufX closes with the membrane plane and with the last LH1 are depicted.

(B) Position of PufX (red) within the complex is shown at the top, and its interacting interfaces are boxed and marked 1–3.

(C) Zoomed-in views of interacting interfaces marked as 1–3 in (B). All interacting residues are shown in sticks and labeled. All interaction distances are shown in Å.

(D) Comparison of interactions at the N terminus of PufX between *Rba. capsulatus* (orange) and its PufX-containing relatives *Rba. sphaeroides* (blue, PDB: 7VOR) and *Rba. veldkampii* (green, PDB: 7DDQ). All amino acids that form interactions with their residues are shown in sticks, and their interacting partners are shown in gray. All interaction distances are shown in Å.

(E) Sequence alignment of PufX polypeptides from those species of *Rhodobacter* with known RC-LH1 assembly. PufX in the species that only produce RC-LH1 monomers are outlined in the green box. Interacting residues depicted in (D) are marked on sequence alignment with arrows. *Rba. capsulatus*, orange; *Rba. sphaeroides*, blue; *Rba. veldkampii* green; first Lys of the transmembrane α-helix, black.

See also Figure S7 and Table S2.

of PufX do not coincide in either their position or affinity (Figure 2E). PufX in *Rba. sphaeroides* dimer forms hydrogen bonds with the other monomer through Asp9 and Arg20 (Figure 2D).[18] It was previously shown that truncation of the 7-residue N terminus of PufX in *Rba. sphaeroides* impaired the core dimerization[28] and that truncation of N-terminal 12 residues resulted in a

Please cite this article in press as: Bracun et al., Cryo-EM structure of a monomeric RC-LH1-PufX supercomplex with high-carotenoid content from *Rhodobacter capsulatus*, Structure (2023), https://doi.org/10.1016/j.str.2023.01.006



CellPress
OPEN ACCESS

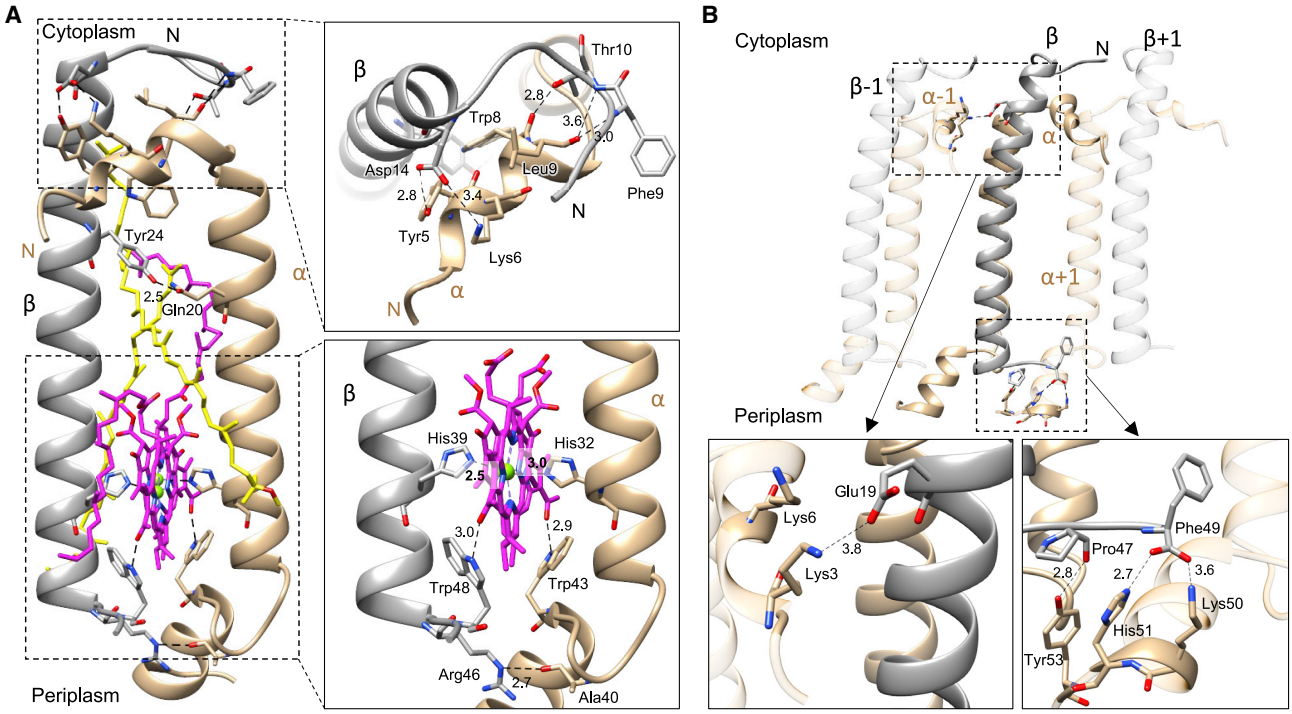


**Figure 3. Interactions of the LH1 antennae**

(A) Intra-subunit LH1 interactions are depicted between protein chains α (brown), β (gray), and associated cofactors (BChls, magenta; carotenoids, yellow). Zoomed-in views are shown in boxes on the right. All interacting residues are shown as sticks and labeled. All interaction distances are shown in Å.

(B) Interactions between neighboring LH1 subunits are depicted. Zoomed-in views are shown in boxes where all interacting residues are shown in sticks and labeled. All interaction distances are shown in Å. Associated pigments are omitted for clarity.

See also Figures S8 and S9 and Tables S3 and S4.

complete loss of dimerization.[27] These results suggested the potential importance of *Rba. sphaeroides* PufX Asp9 in the dimerization of the RC-LH1 core complex. Additional connections between two monomers in the dimer are provided by interactions between PufX Arg20, which is conserved in all dimers, and the other RC-H, as well as several interactions between PufX main-chain peptide bonds close to the N terminus and the other LH1 (Figures 2D and 2E).[18] Whether the specific interaction mediated by the highly conserved Arg20 is crucial for the dimerization of RC-LH1-PufX requires further investigation.

## The LH1 architecture

Another striking difference between *Rba. capsulatus* and *Rba. veldkampii* RC-LH1-PufX architectures is the number of carotenoid molecules per LH1 αβ heterodimer. *Rba. veldkampii* RC-LH1-PufX contains one carotenoid per LH1 αβ heterodimer, the same as many other purple photosynthetic bacteria.[9,11,12,15,19] In contrast, each LH1 αβ heterodimer of *Rba. capsulatus* RC-LH1-PufX possesses two carotenoid molecules in addition to two BChls (Figure 3A), consistent with previous biochemical analysis[39,45] and resembling the RC-LH1 monomer and dimer from *Rba. sphaeroides*.[18,20,21,24,25] The exceptions are LH1-13 and LH1-14 subunits with only one carotenoid modeled due to poor local density (see details below), as well as the LH1-15 subunit adjacent to the LH1 opening, which contains no carotenoid. The two carotenoids were assigned as *trans*-spheroidenes based on their electron densities, abundance in *Rba. capsulatus*,[48] and spectral properties (Figure S1C). The commonly identified carotenoid is close to the inner edge of the LH1 ring, whereas the additional carotenoid is close to the outer edge (Figure S8A). No strong non-covalent interactions were found between carotenoids with the LH1 subunits, and their association is presumably formed by van der Waals contacts and steric restraints (Figure S8B; Table S3). On one hand, the extra carotenoids could enhance the light harvesting and photoprotection capacities of RC-LH1; on the other hand, they could impede quinone/quinol passage through the small pores formed between two adjacent LH1 subunits.[9,12,19] This highlights the importance of the PufX-mediated gap within LH1 in tunneling quinone/quinol passage across the LH1 array. It remains unclear what determined the number and association of carotenoids within the LH1 αβ heterodimer given that the LH1 αβ-apoproteins are highly conserved in both sequence and structure from distinct species regardless of their copy numbers of carotenoids per LH1 αβ heterodimer (Figures S8C and S9). It was previously shown that the mutation of α-Ser2, α-Trp8, or α-Asp12 residues could alter the number of carotenoids associated with LH1 in *Rba. capsulatus*.[39,49] However, the interactions between these residues and carotenoids are not apparent from the structural model alone, and these residues are conserved in *Rba. veldkampii* (Figures S8C and S9).

The inner LH1 α-apoprotein consists of a transmembrane α-helix, an amphiphilic N-terminal $3_{10}$-helix parallel to the membrane plane, and a short C-terminal α-helix that sticks out of the

Please cite this article in press as: Bracun et al., Cryo-EM structure of a monomeric RC-LH1-PufX supercomplex with high-carotenoid content from *Rhodobacter capsulatus*, Structure (2023), https://doi.org/10.1016/j.str.2023.01.006



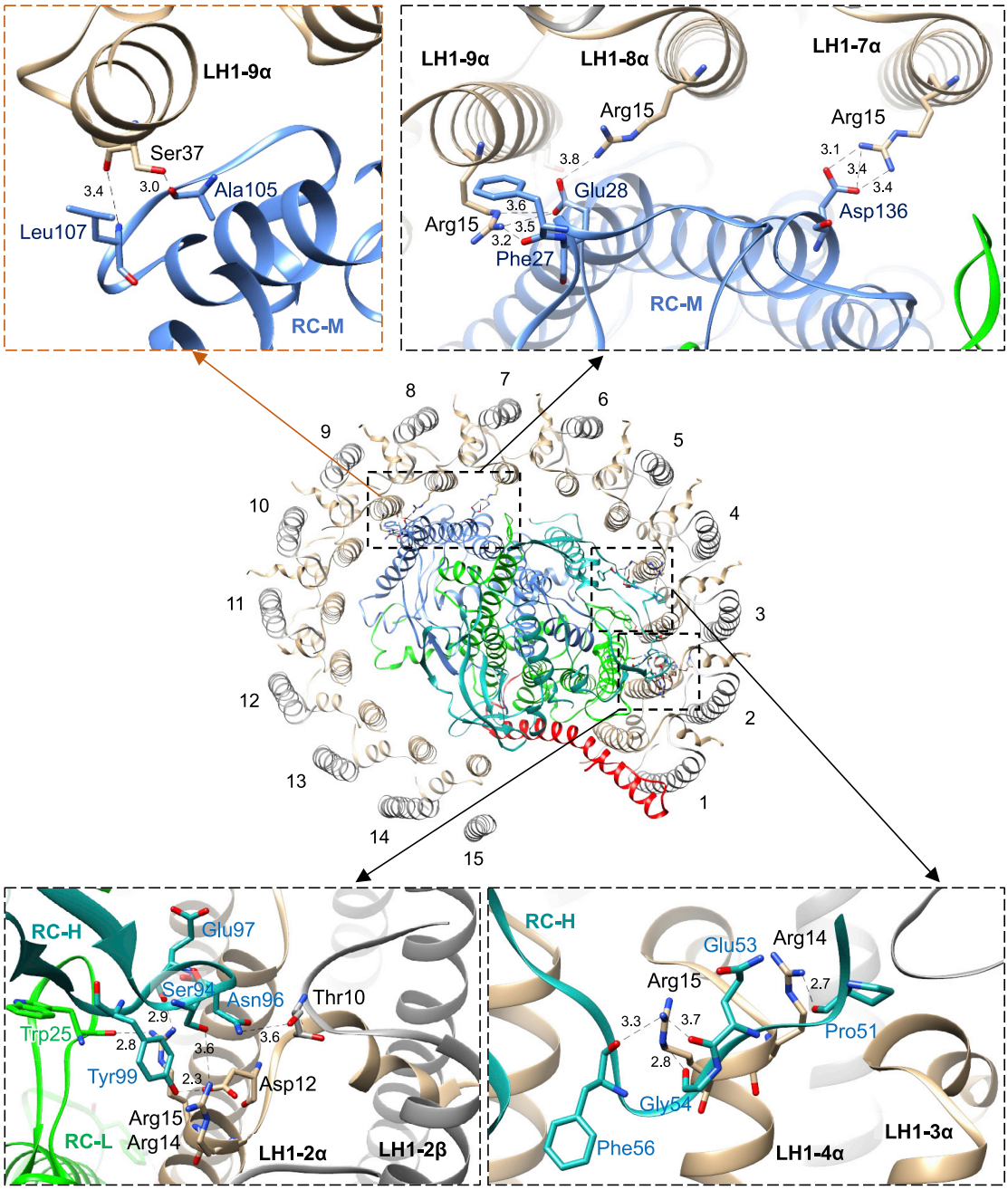


**Figure 4. Interactions of RC with the LH1 ring**

The complex is shown as viewed from the cytoplasmic side of the membrane and is color coded as in Figure 1. Interaction interfaces are marked by boxes, and their zoom-in views are shown in boxes. Black boxes represent views close to the cytoplasmic surface of the complex, and orange boxes represent views close to the periplasmic surface. Interacting residues are shown in sticks and labeled. All interaction distances are shown in Å (see also Table S5). Cofactors are omitted for clarity. See also Table S5.

membrane into the periplasm. The LH1 α-chain coordinates the central $Mg^{2+}$ atom of adjacent BChl *a* by its His32 residue, and the Trp43 residue is hydrogen bonded to the keto-oxygen of BChl *a* (Figure 3A). The outer LH1 β-apoprotein consists of a single transmembrane α-helix that rises above its partner's $3_{10}$-helix on the cytoplasmic side of the membrane near the N terminus but is shorter than the α-chain on the periplasmic side. The His39 and Trp48 residues of the LH1 β-chain coordinate the BChl $Mg^{2+}$ and keto-oxygen atoms, respectively.

The cryo-EM structure reveals extensive intra- and inter-molecular interactions of LH1 subunits (Table S4). Within an individual LH1 αβ-heterodimer, the LH1 α- and β-apoproteins interconnect mostly through their N- and C-terminal regions, in addition to the interaction interface formed by the two

Please cite this article in press as: Bracun et al., Cryo-EM structure of a monomeric RC-LH1-PufX supercomplex with high-carotenoid content from *Rhodobacter capsulatus*, Structure (2023), https://doi.org/10.1016/j.str.2023.01.006



CellPress
OPEN ACCESS

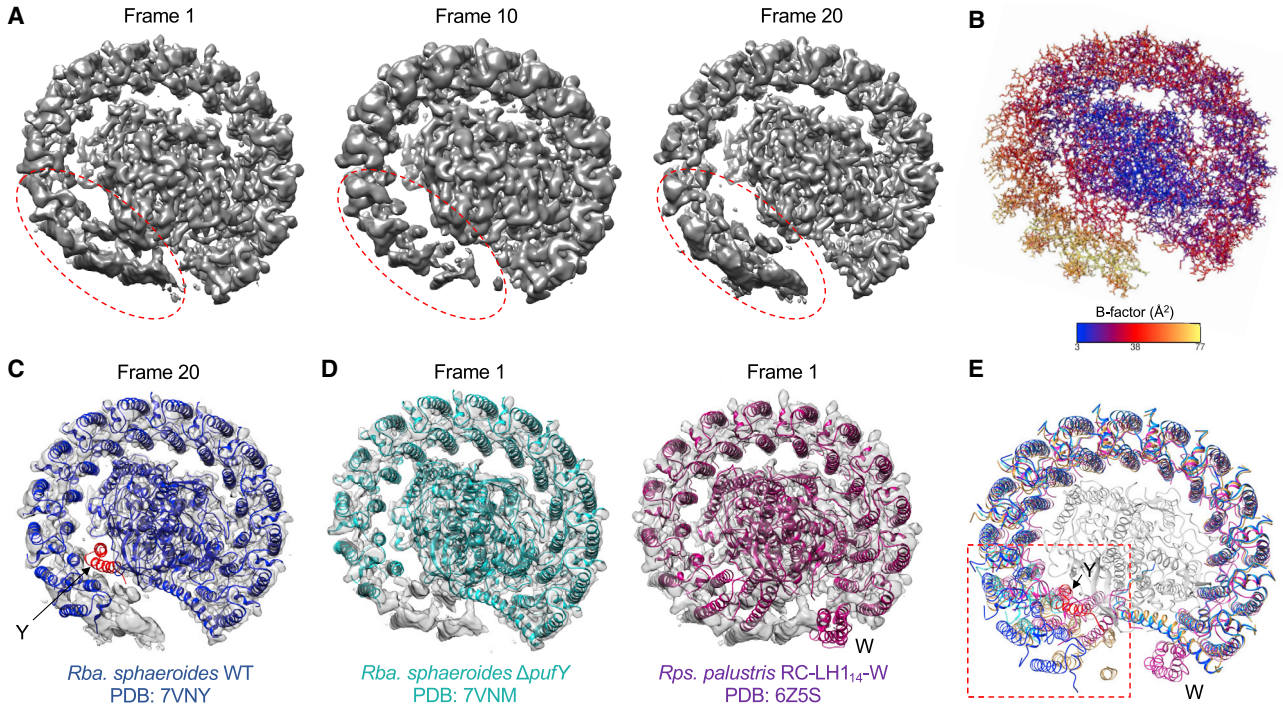


**Figure 5. Structural flexibility of the LH1 ring**

(A) 3D variability analysis of RC-LH1 shows the "breathing" process of the LH1 architecture in a most closed form (left, frame 1), in an intermediate form (middle, frame 10), and in a more open form (right, frame 20), due to the organizational flexibility of the last LH1 subunits. See also Video S1.

(B) The *Rba. capsulatus* RC-LH1 structure is shown as lines, colored by B-factor. Higher B-factor values were observed at the last LH1 subunits, indicating their structural flexibility within the RC-LH1 architecture. The coloring according to B-factor was conducted by using UCSF Chimera.

(C) Superimposition of the cryo-EM map of *Rba. capsulatus* RC-LH1 in the most open form and *Rba. sphaeroides* WT RC-LH1 monomer structure containing a PufY between the RC and LH1 (PDB: 7VNY).

(D) Superimposition of the cryo-EM map of *Rba. capsulatus* RC-LH1 in the most closed form, *Rba. sphaeroides* Δ*pufY* RC-LH1 monomer (left, PDB: 7VNM), and *Rps. palustris* RC-LH1$_{14}$-W containing a transmembrane polypeptide W (right, PDB: 6Z5S).

(E) Comparison of the *Rba. capsulatus* RC-LH1 (orange), *Rba sphaeroides* WT RC-LH1 monomer (blue, PufY indicated in red), *Rba. sphaeroides* Δ*pufY* RC-LH1 monomer (light blue) models, and *Rps. palustris* RC-LH1$_{14}$-W (pink). The red square indicates the last LH1 subunits that exhibit a high structural variability, which appears to be a general feature of the RC-LH1 complexes. The PufY peptide clashes with the LH1 subunits of *Rba capsulatus, Rba. sphaeroides* Δ*pufY*, and *Rps. palustris* RC-LH1 structures. Note that the *Rba. veldkampii* RC-LH1 structurally resembles *Rba. capsulatus* RC-LH1 at this highlighted region and thus is not included in this analysis.

associated BChls and one hydrogen bond formed by α-Gln20 and β-Tyr24 (Figure 3A). β-Asp14 forms a hydrogen bond and a salt bridge with α-Tyr5 and α-Lys6, respectively; α-Trp8 and α-Leu9 main-chain oxygen atoms form hydrogen bonds with the side chain of β-Thr10 and main-chain nitrogen of β-Phe9; β-Arg46 participates in the intra-LH1 interaction near the C terminus by interacting with the main chain oxygen of α-Ala40 (Figure 3A).

Both short helices at the termini of the LH1 α-apoprotein interact with the paired β-apoprotein and the β-apoprotein of neighboring LH1 subunits, facilitating the LH1 intra- and inter-subunit interactions (Figure 3B), as found in other RC-LH1 complexes.[15,18,19,21] Two neighboring LH1 αβ-heterodimers form extensive interactions including the overlap of BChls, salt bridges between α-Lys3 (or α-Lys6) and β-Glu18 at the cytoplasmic side, and hydrogen bonds between α-Lys50, α-His51, and β-Phe49 as well as between α-Tyr53 and β-Pro47 at the periplasmic side (Figure 3B). Collectively, these interactions provide the foundation for the formation of a rigid LH1 ring architecture and integration of pigments within the LH1.

## RC-LH1 interactions

Out of 15 LH1 antennae surrounding the RC, five were found to directly interact with the RC, forming two large interaction interfaces. One of those is made of LH1 subunits 2 and 4 and the other of LH1 subunits 7–9 (Figure 4). The main interacting residues are Arg15 and Ser37 of the LH1 α-chain. They participate in forming all the hydrogen bonds and salt bridges between LH1-7, LH1-8, and LH1-9 and the M subunit of the RC, as well as the majority of hydrogen bonds and salt bridges between LH1-2 and LH1-4 and the subunits H and L of the RC, in which case they are joined by Arg14 (Figure 4; Table S5). Only one LH1 β-chain directly interacts with the RC, and that is the β-chain of LH1 subunit 2 due to the proximity of its main-chain peptide bond of Thr10 to the H subunit Asn96 residue. It is important to note here that LH1 subunit 1 connects with the RC indirectly by interacting with PufX at its N-terminal region, while its C-terminal region binds to the L subunit of the RC, as discussed below.

LH1 subunits 10–15 do not form stable interactions with the central RC and are presumed to be more flexible based on the cryo-EM density map (Figure S2F). 3D variability analysis

Please cite this article in press as: Bracun et al., Cryo-EM structure of a monomeric RC-LH1-PufX supercomplex with high-carotenoid content from *Rhodobacter capsulatus*, Structure (2023), https://doi.org/10.1016/j.str.2023.01.006



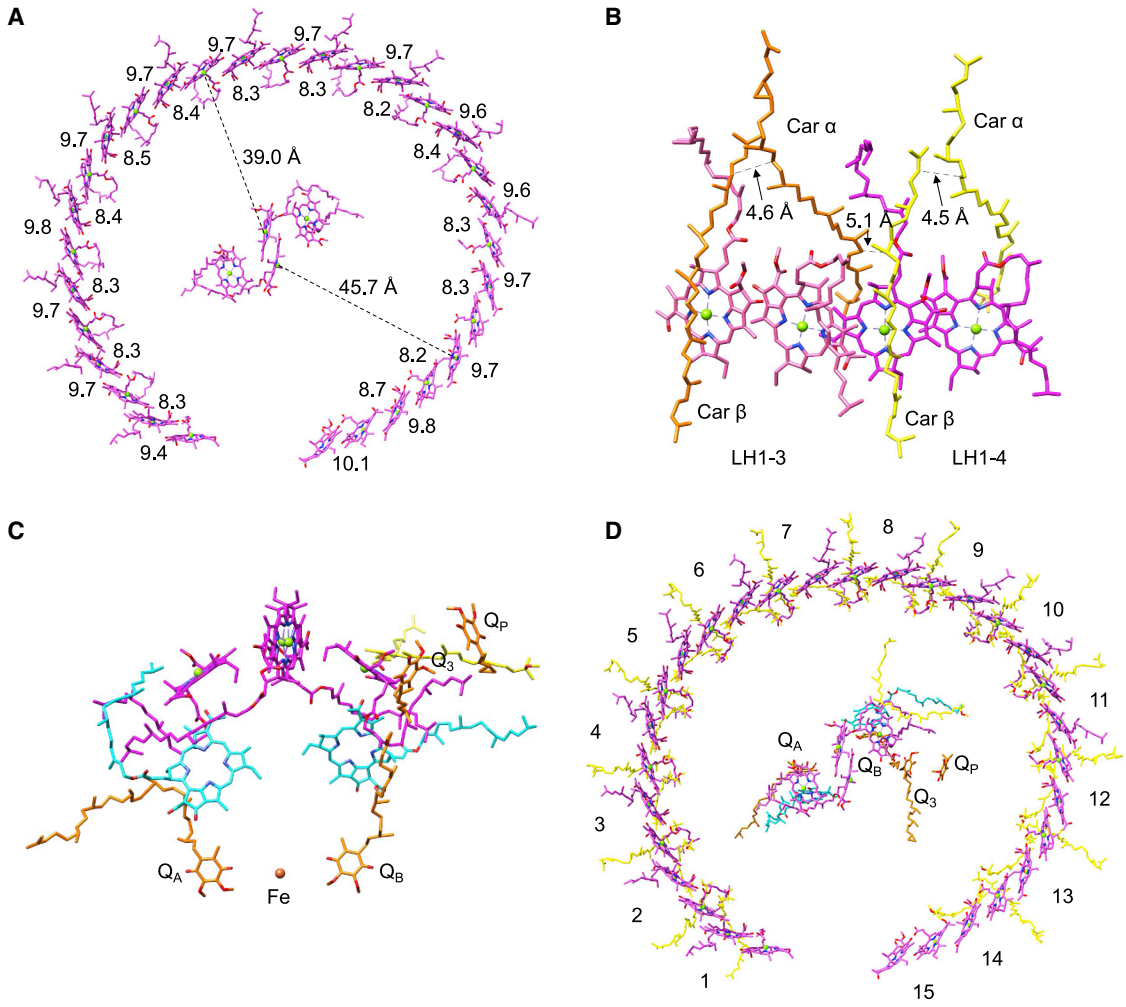


**Figure 6. Pigment composition of RC-LH1-PufX complex from *Rba. capsulatus***

(A) Mg-Mg distances of BChls are depicted on a periplasmic view. The shortest and the longest distance from LH1-associated BChls to the special pair are marked. The distances between BChls belonging to the same LH1 subunit are marked on the outside of the ring, and the distances of BChls of the neighboring LH1 subunits are marked on the inside. All distances are measured in Å.

(B) Shortest distances between carotenoids of LH1 subunits 4 and 5 are shown.

(C) Arrangement of the cofactors associated with the RC.

(D) Positions of pigments and electron carriers as viewed from the periplasmic side of the membrane. Color scheme is the same as that in Figure 1. LH1 antenna numbers and quinones are marked.

See also Figures S10–S12.

of the cryo-EM density maps confirmed that the last LH1 subunits display higher degrees of structural flexibility compared with other LH1 subunits within the *Rba. capsulatus* RC-LH1, resulting in varying levels of the LH1 opening and a dynamic or "breathing" architecture of the LH1 ring (Figure 5A; Video S1). This structural flexibility was further supported by the analysis of temperature B-factors (Figure 5B). It is presumably that the RC-LH1 complex in native photosynthetic membranes has a dynamic LH1 surrounding, which may play a role in modulating quinone/quinol exchange to the $Q_B$ site and needs further experimental verifications.

Interestingly, the most open form of *Rba. capsulatus* RC-LH1 has a similar LH1 arrangement as the *Rba. sphaeroides* WT RC-LH1 monomer (Figure 5C), in which the transmembrane polypeptide PufY sits between the RC and LH1 and creates extra space between LH1-13/14 and the RC.[18] By contrast, the most closed form appears to fit the *Rba. sphaeroides* Δ*pufY* RC-LH1 monomer structure that lacks the PufY-mediated physical separation between the RC and LH1[18] and *Rps. palustris* RC-$LH1_{14}$-W with a closed LH1 association to the RC[11] (Figure 5D). Moreover, deletion of PufY destabilizes the last 3–4 LH1 subunits in *Rba. sphaeroides* RC-LH1, causing their poor densities.[18,25] It is likely that the structural flexibility of LH1 subunits near the LH1 opening is a general assembly feature of the RC-LH1 core complexes with an open LH1 ring, which require specific interactions between their final LH1 subunits and the RC (either direct or indirect through other structural elements like PufY), to enhance the LH1 architectural rigidity (Figure 5E).[11,17–21]

### Arrangement of cofactors

A total of 30 BChls *a* were identified in the LH1 ring. The intra-subunit Mg-Mg distances range from 9.4 to 10.1 Å, whereas the Mg-Mg distances of BChls associated with neighboring LH1 subunits are slightly shorter, ranging from 8.2 to 8.7 Å. The distance from an LH1 BChl to one of the special pair BChls in the RC ranges between 39 and 45.7 Å (Figure 6A). Except for LH1-15, each LH1 is presumed to host two *trans*-spheroidene carotenoids. Out of the 28 expected carotenoids, 26 were modeled. The outer carotenoids in LH1-14 and LH1-13 subunits are missing due to their relatively poor density of the area, presumably originating from structural flexibility (Figures 1A and S2F). The approximate shortest distances between the two carotenoids within the LH1 subunits range from 3.6 to 5.5 Å (Figures 6B and S10).

The cofactors of the RC include two BChls *a* making up the special pair dimer, two accessory BChls *a*, two BPheos *a*, a *cis*-carotenoid, a primary quinone $Q_A$ and a secondary quinone $Q_B$, which are both modeled as ubiquinone 10, as well as a non-heme iron (Figure 6C). Two additional quinones, named $Q_3$ and $Q_P$, were modeled outside the RC (Figures 6C and 6D). $Q_3$ locates outside of the $Q_B$ site oriented with its head toward $Q_B$.[9,13,18,19,50] $Q_P$ (also as $Q_6$ in Bracun et al.[19] and $Q_2$ in Swainsbury et al.[11]) is proposed to be near $Q_3$ but in an opposite orientation facing the periplasm.[11,19,20,25] While its tail density could not be clearly traced, a planar density that fits a quinone head was undoubtedly identified to be sandwiched between aromatic residues (Figure S11). These surrounding aromatic residues are conserved in all reported RC-LH1 structures (Figure S12), suggesting their potential functions in facilitating quinone transport through aromatic ring-aliphatic ring interactions.[51]

In summary, the cryo-EM structure of *Rba. capsulatus* RC-LH1-PufX unveils unprecedented architectural details of the unique photosynthetic RC-LH1 core supercomplex, representing an intermediate structure between *Rba. veldkampii* and *Rba. sphaeroides* RC-LH1-PufX complexes. The study provides insights into the molecular basis of light harvesting and quinone diffusion in *Rba. capsulatus* RC-LH1-PufX and expands our understanding of the structural diversity and flexibility of bacterial photosynthetic core complexes, which is desirable for different phototrophic species to optimize photosynthetic performance in their specific ecological niches.

## STAR★METHODS

Detailed methods are provided in the online version of this paper and include the following:



### SUPPLEMENTAL INFORMATION

Supplemental information can be found online at https://doi.org/10.1016/j.str.2023.01.006.


### ACKNOWLEDGMENTS

We thank T. Uchikubo, R. Akasaka, and H. Ehara for their help with cryo-EM data collection and analysis and Liverpool Biomedical Electron Microscopy Unit for providing technical assistance and provision for microscopic imaging. We thank Dr Daniel Canniffe (University of Liverpool, UK) for kind support in this project. All cryo-EM data were collected at the cryo-EM facility of the RIKEN Center for Biosystems Dynamics Research (Yokohama). This work was supported by the National Key R&D Program of China (2021YFA0909600); the National Natural Science Foundation of China (32070109); the Royal Society (URF\R\180030, RGF\EA\181061, and RGF\EA\180233 to L.-N.L.); and the Biotechnology and Biological Sciences Research Council Grant (BB\W001012\1, BB\V009729\1, and BB\R003890\1 to L.-N.L.). This work was partially supported by grants from JSPS\MEXT KAKENHI (JP22H02564 to A.Y.); Platform Project for Supporting Drug Discovery and Life Science Research (Basis for Supporting Innovative Drug Discovery and Life Science Research [BINDS]) from AMED (JP21am0101082 to M.S.); RIKEN Pioneering Projects "Biology of Intracellular Environments" (to M.S.); and RIKEN BDR Structural Cell Biology Project (to M.S.). L.B. was supported by a Liverpool-Riken International PhD Studentship.


### AUTHOR CONTRIBUTIONS

Conceptualization, L.-N.L.; methodology, L.B., A.Y., and B.M.C.; investigation, L.B., A.Y., and B.M.C.; writing – original draft, L.B. and L.-N.L.; writing – review & editing, L.B., A.Y., B.M.C., M.S., and L.-N.L.; funding acquisition, M.S. and L.-N.L.; supervision, A.Y., M.S., and L.-N.L.

### DECLARATION OF INTERESTS

The authors declare no competing interests.


Received: October 7, 2022
Revised: December 30, 2022
Accepted: January 11, 2023
Published: February 3, 2023


### REFERENCES


1. Mullineaux, C.W., and Liu, L.N. (2020). Membrane dynamics in phototrophic bacteria. Annu. Rev. Microbiol. *74*, 633–654. https://doi.org/10.1146/annurev-micro-020518-120134.
2. Cogdell, R.J., Gall, A., and Köhler, J. (2006). The architecture and function of the light-harvesting apparatus of purple bacteria: from single molecules to in vivo membranes. Q. Rev. Biophys. *39*, 227–324. https://doi.org/10.1017/S0033583506004434.
3. Liu, L.N., and Scheuring, S. (2013). Investigation of photosynthetic membrane structure using atomic force microscopy. Trends Plant Sci. *18*, 277–286. https://doi.org/10.1016/j.tplants.2013.03.001.
4. Jones, M.R. (2021). Photosynthesis | purple bacteria: photosynthetic reaction centers. In Encyclopedia of Biological Chemistry III, Third Edition, J. Jez, ed. (Elsevier), pp. 315–332. https://doi.org/10.1016/B978-0-12-809633-8.21540-9.
5. Miller, L.C., Martin, D.S., Liu, L.N., and Canniffe, D.P. (2020). Composition, organisation and function of purple photosynthetic machinery. In Microbial Photosynthesis, Q. Wang, ed. (Springer Singapore), pp. 73–114. https://doi.org/10.1007/978-981-15-3110-1_4.

6. Singharoy, A., Maffeo, C., Delgado-Magnero, K.H., Swainsbury, D.J.K., Sener, M., Kleinekathöfer, U., Vant, J.W., Nguyen, J., Hitchcock, A., Isralewitz, B., et al. (2019). Atoms to phenotypes: molecular design principles of cellular energy metabolism. Cell *179*, 1098–1111.e23. https://doi.org/10.1016/j.cell.2019.10.021.

7. Gardiner, A.T., Nguyen-Phan, T.C., and Cogdell, R.J. (2020). A comparative look at structural variation among RC-LH1 'Core' complexes present in anoxygenic phototrophic bacteria. Photosynth. Res. *145*, 83–96. https://doi.org/10.1007/s11120-020-00758-3.

8. Niwa, S., Yu, L.J., Takeda, K., Hirano, Y., Kawakami, T., Wang-Otomo, Z.Y., and Miki, K. (2014). Structure of the LH1-RC complex from *Thermochromatium tepidum* at 3.0 Å. Nature *508*, 228–232. https://doi.org/10.1038/nature13197.

9. Yu, L.J., Suga, M., Wang-Otomo, Z.Y., and Shen, J.R. (2018). Structure of photosynthetic LH1-RC supercomplex at 1.9 Å resolution. Nature *556*, 209–213. https://doi.org/10.1038/s41586-018-0002-9.

10. Tani, K., Kanno, R., Makino, Y., Hall, M., Takenouchi, M., Imanishi, M., Yu, L.J., Overmann, J., Madigan, M.T., Kimura, Y., et al. (2020). Cryo-EM structure of a $Ca^{2+}$-bound photosynthetic LH1-RC complex containing multiple alphabeta-polypeptides. Nat. Commun. *11*, 4955. https://doi.org/10.1038/s41467-020-18748-3.

11. Swainsbury, D.J.K., Qian, P., Jackson, P.J., Faries, K.M., Niedzwiedzki, D.M., Martin, E.C., Farmer, D.A., Malone, L.A., Thompson, R.F., Ranson, N.A., et al. (2021). Structures of *Rhodopseudomonas palustris* RC-LH1 complexes with open or closed quinone channels. Sci. Adv. *7*, eabe2631. https://doi.org/10.1126/sciadv.abe2631.

12. Qian, P., Croll, T.I., Swainsbury, D.J.K., Castro-Hartmann, P., Moriarty, N.W., Sader, K., and Hunter, C.N. (2021). Cryo-EM structure of the *Rhodospirillum rubrum* RC-LH1 complex at 2.5 Å. Biochem. J. *478*, 3253–3263. https://doi.org/10.1042/BCJ20210511.

13. Tani, K., Kanno, R., Ji, X.C., Hall, M., Yu, L.J., Kimura, Y., Madigan, M.T., Mizoguchi, A., Humbel, B.M., and Wang-Otomo, Z.Y. (2021). Cryo-EM structure of the photosynthetic LH1-RC complex from *Rhodospirillum rubrum*. Biochemistry *60*, 2483–2491. https://doi.org/10.1021/acs.biochem.1c00360.

14. Qian, P., Gardiner, A.T., Šímová, I., Naydenova, K., Croll, T.I., Jackson, P.J., Nupur, Kloz, M., Kloz, M., Čubáková, P., Kuzma, M., et al. (2022). 2.4-A structure of the double-ring *Gemmatimonas phototrophica* photosystem. Sci. Adv. *8*, eabk3139. https://doi.org/10.1126/sciadv.abk3139.

15. Qian, P., Siebert, C.A., Wang, P., Canniffe, D.P., and Hunter, C.N. (2018). Cryo-EM structure of the *Blastochloris viridis* LH1-RC complex at 2.9 Å. Nature *556*, 203–208. https://doi.org/10.1038/s41586-018-0014-5.

16. Roszak, A.W., Howard, T.D., Southall, J., Gardiner, A.T., Law, C.J., Isaacs, N.W., and Cogdell, R.J. (2003). Crystal structure of the RC-LH1 core complex from *Rhodopseudomonas palustris*. Science *302*, 1969–1972. https://doi.org/10.1126/science.1088892.

17. Xin, Y., Shi, Y., Niu, T., Wang, Q., Niu, W., Huang, X., Ding, W., Yang, L., Blankenship, R.E., Xu, X., and Sun, F. (2018). Cryo-EM structure of the RC-LH core complex from an early branching photosynthetic prokaryote. Nat. Commun. *9*, 1568. https://doi.org/10.1038/s41467-018-03881-x.

18. Cao, P., Bracun, L., Yamagata, A., Christianson, B.M., Negami, T., Zou, B., Terada, T., Canniffe, D.P., Shirouzu, M., Li, M., and Liu, L.N. (2022). Structural basis for the assembly and quinone transport mechanisms of the dimeric photosynthetic RC-LH1 supercomplex. Nat. Commun. *13*, 1977. https://doi.org/10.1038/s41467-022-29563-3.

19. Bracun, L., Yamagata, A., Christianson, B.M., Terada, T., Canniffe, D.P., Shirouzu, M., and Liu, L.N. (2021). Cryo-EM structure of the photosynthetic RC-LH1-PufX supercomplex at 2.8- Å resolution. Sci. Adv. *7*, eabf8864. https://doi.org/10.1126/sciadv.abf8864.

20. Tani, K., Nagashima, K.V.P., Kanno, R., Kawamura, S., Kikuchi, R., Hall, M., Yu, L.J., Kimura, Y., Madigan, M.T., Mizoguchi, A., et al. (2021). A previously unrecognized membrane protein in the *Rhodobacter sphaeroides* LH1-RC photocomplex. Nat. Commun. *12*, 6300. https://doi.org/10.1038/s41467-021-26561-9.

21. Qian, P., Swainsbury, D.J.K., Croll, T.I., Salisbury, J.H., Martin, E.C., Jackson, P.J., Hitchcock, A., Castro-Hartmann, P., Sader, K., and Hunter, C.N. (2021). Cryo-EM structure of the monomeric *Rhodobacter sphaeroides* RC-LH1 core complex at 2.5 Å. Biochem. J. *478*, 3775–3790. https://doi.org/10.1042/BCJ20210631.

22. Crouch, L.I., and Jones, M.R. (2012). Cross-species investigation of the functions of the Rhodobacter PufX polypeptide and the composition of the RC-LH1 core complex. Biochim. Biophys. Acta *1817*, 336–352. https://doi.org/10.1016/j.bbabio.2011.10.009.

23. Semchonok, D.A., Siponen, M.I., Tüting, C., Charras, Q., Kyrilis, F.L., Hamdi, F., Sadian, Y., Jungas, C., and Kastritis, P.L. (2022). Cryo-EM structure of the *Rhodobaca bogoriensis* RC-LH1-PufX dimeric complex at 2.9 Å. Preprint at bioRxiv. https://doi.org/10.1101/2022.02.25.481955.

24. Qian, P., Croll, T.I., Hitchcock, A., Jackson, P.J., Salisbury, J.H., Castro-Hartmann, P., Sader, K., Swainsbury, D.J.K., and Hunter, C.N. (2021). Cryo-EM structure of the dimeric *Rhodobacter sphaeroides* RC-LH1 core complex at 2.9 Å: the structural basis for dimerisation. Biochem. J. *478*, 3923–3937. https://doi.org/10.1042/BCJ20210696.

25. Tani, K., Kanno, R., Kikuchi, R., Kawamura, S., Nagashima, K.V.P., Hall, M., Takahashi, A., Yu, L.J., Kimura, Y., Madigan, M.T., et al. (2022). Asymmetric structure of the native *Rhodobacter sphaeroides* dimeric LH1-RC complex. Nat. Commun. *13*, 1904. https://doi.org/10.1038/s41467-022-29453-8.

26. Qian, P., Martin, E.C., Ng, I.W., and Hunter, C.N. (2017). The C-terminus of PufX plays a key role in dimerisation and assembly of the reaction center light-harvesting 1 complex from *Rhodobacter sphaeroides*. Biochim. Biophys. Acta. Bioenerg. *1858*, 795–803. https://doi.org/10.1016/j.bbabio.2017.06.001.

27. Ratcliffe, E.C., Tunnicliffe, R.B., Ng, I.W., Adams, P.G., Qian, P., Holden-Dye, K., Jones, M.R., Williamson, M.P., and Hunter, C.N. (2011). Experimental evidence that the membrane-spanning helix of PufX adopts a bent conformation that facilitates dimerisation of the *Rhodobacter sphaeroides* RC-LH1 complex through N-terminal interactions. Biochim. Biophys. Acta *1807*, 95–107. https://doi.org/10.1016/j.bbabio.2010.10.003.

28. Francia, F., Wang, J., Zischka, H., Venturoli, G., and Oesterhelt, D. (2002). Role of the N- and C-terminal regions of the PufX protein in the structural organization of the photosynthetic core complex of *Rhodobacter sphaeroides*. Eur. J. Biochem. *269*, 1877–1885. https://doi.org/10.1046/j.1432-1033.2002.02834.x.

29. Brinkmann, H., Göker, M., Koblížek, M., Wagner-Döbler, I., and Petersen, J. (2018). Horizontal operon transfer, plasmids, and the evolution of photosynthesis in Rhodobacteraceae. ISME J. *12*, 1994–2010. https://doi.org/10.1038/s41396-018-0150-9.

30. Bauer, C., Buggy, J., and Mosley, C. (1993). Control of photosystem genes in *Rhodobacter capsulatus*. Trends Genet. *9*, 56–60. https://doi.org/10.1016/0168-9525(93)90188-N.

31. Spanoghe, J., Vermeir, P., and Vlaeminck, S.E. (2021). Microbial food from light, carbon dioxide and hydrogen gas: kinetic, stoichiometric and nutritional potential of three purple bacteria. Bioresour. Technol. *337*, 125364. https://doi.org/10.1016/j.biortech.2021.125364.

32. Gubellini, F., Francia, F., Turina, P., Lévy, D., Venturoli, G., and Melandri, B.A. (2007). Heterogeneity of photosynthetic membranes from *Rhodobacter capsulatus*: size dispersion and ATP synthase distribution. Biochim. Biophys. Acta *1767*, 1340–1352. https://doi.org/10.1016/j.bbabio.2007.08.007.

33. Sturgis, J.N., and Niedermann, R.A. (1996). The effect of different levels of the B800-850 light-harvesting complex on intracytoplasmic membrane development in *Rhodobacter sphaeroides*. Arch. Microbiol. *165*, 235–242.

34. Hunter, C.N., Pennoyer, J.D., Sturgis, J.N., Farrelly, D., and Niederman, R.A. (1988). Oligomerization states and associations of light-harvesting pigment-protein complexes of *Rhodobacter sphaeroides* as analyzed by lithium dodecyl sulfate-polyacrylamide gel electrophoresis. Biochemistry *27*, 3459–3467. https://doi.org/10.1021/bi00409a050.

35. Scheuring, S., Nevo, R., Liu, L.N., Mangenot, S., Charuvi, D., Boudier, T., Prima, V., Hubert, P., Sturgis, J.N., and Reich, Z. (2014). The architecture of *Rhodobacter sphaeroides* chromatophores. Biochim. Biophys. Acta *1837*, 1263–1270. https://doi.org/10.1016/j.bbabio.2014.03.011.

36. Tucker, J.D., Siebert, C.A., Escalante, M., Adams, P.G., Olsen, J.D., Otto, C., Stokes, D.L., and Hunter, C.N. (2010). Membrane invagination in *Rhodobacter*

*sphaeroides* is initiated at curved regions of the cytoplasmic membrane, then forms both budded and fully detached spherical vesicles. Mol. Microbiol. *76*, 833–847. https://doi.org/10.1111/j.1365-2958.2010.07153.x.

37. Noble, J.M., Lubieniecki, J., Savitzky, B.H., Plitzko, J., Engelhardt, H., Baumeister, W., and Kourkoutis, L.F. (2018). Connectivity of centermost chromatophores in *Rhodobacter sphaeroides* bacteria. Mol. Microbiol. *109*, 812–825. https://doi.org/10.1111/mmi.14077.
38. Liu, L.N., Sturgis, J.N., and Scheuring, S. (2011). Native architecture of the photosynthetic membrane from *Rhodobacter veldkampii*. J. Struct. Biol. *173*, 138–145. https://doi.org/10.1016/j.jsb.2010.08.010.
39. Babst, M., Albrecht, H., Wegmann, I., Brunisholz, R., and Zuber, H. (1991). Single amino acid substitutions in the B870 α and β light-harvesting polypeptides of *Rhodobacter capsulatus*. Structural and spectral effects. Eur. J. Biochem. *202*, 277–284. https://doi.org/10.1111/j.1432-1033.1991.tb16373.x.
40. Zuber, H., Brunisholz, R., and Sidler, W. (1987). Chapter 11 Structure and function of light-harvesting pigment-protein complexes. In New Comprehensive Biochemistry, J. Amesz, ed. (Elsevier), pp. 233–271. https://doi.org/10.1016/S0167-7306(08)60142-8.
41. Suresh, G., Lodha, T.D., Indu, B., Sasikala, C., and Ramana, C.V. (2019). Taxogenomics resolves conflict in the genus rhodobacter: a two and half decades pending thought to reclassify the genus rhodobacter. Front. Microbiol. *10*, 2480. https://doi.org/10.3389/fmicb.2019.02480.
42. Axelrod, H.L., Abresch, E.C., Okamura, M.Y., Yeh, A.P., Rees, D.C., and Feher, G. (2002). X-ray structure determination of the cytochrome c2: reaction center electron transfer complex from *Rhodobacter sphaeroides*. J. Mol. Biol. *319*, 501–515. https://doi.org/10.1016/S0022-2836(02)00168-7.
43. Barz, W.P., Verméglio, A., Francia, F., Venturoli, G., Melandri, B.A., and Oesterhelt, D. (1995). Role of the PufX protein in photosynthetic growth of *Rhodobacter sphaeroides*. 2. PufX is required for efficient ubiquinone/ubiquinol exchange between the reaction center QB site and the cytochrome *bc*1 complex. Biochemistry *34*, 15248–15258. https://doi.org/10.1021/bi00046a033.
44. Siebert, C.A., Qian, P., Fotiadis, D., Engel, A., Hunter, C.N., and Bullough, P.A. (2004). Molecular architecture of photosynthetic membranes in *Rhodobacter sphaeroides*: the role of PufX. EMBO J. *23*, 690–700. https://doi.org/10.1038/sj.emboj.7600092.
45. Lilburn, T.G., Haith, C.E., Prince, R.C., and Beatty, J.T. (1992). Pleiotropic effects of pufX gene deletion on the structure and function of the photosynthetic apparatus of *Rhodobacter capsulatus*. Biochim. Biophys. Acta *1100*, 160–170. 0005-2728(92)90077-F [pii].
46. Olsen, J.D., Martin, E.C., and Hunter, C.N. (2017). The PufX quinone channel enables the light-harvesting 1 antenna to bind more carotenoids for light collection and photoprotection. FEBS Lett. *591*, 573–580. https://doi.org/10.1002/1873-3468.12575.
47. Francia, F., Wang, J., Venturoli, G., Melandri, B.A., Barz, W.P., and Oesterhelt, D. (1999). The reaction center-LH1 antenna complex of Rhodobacter sphaeroides contains one PufX molecule which is involved in dimerization of this complex. Biochemistry *38*, 6834–6845. https://doi.org/10.1021/bi982891h.
48. Gerjets, T., Steiger, S., and Sandmann, G. (2009). Catalytic properties of the expressed acyclic carotenoid 2-ketolases from *Rhodobacter capsulatus* and *Rubrivivax gelatinosus*. Biochim. Biophys. Acta *1791*, 125–131. https://doi.org/10.1016/j.bbalip.2008.12.006.
49. Aklujkar, M., and Beatty, J.T. (2005). The PufX protein of Rhodobacter capsulatus affects the properties of bacteriochlorophyll a and carotenoid pigments of light-harvesting complex 1. Arch. Biochem. Biophys. *443*, 21–32. https://doi.org/10.1016/j.abb.2005.08.018.
50. Kawakami, T., Yu, L.J., Liang, T., Okazaki, K., Madigan, M.T., Kimura, Y., and Wang-Otomo, Z.Y. (2021). Crystal structure of a photosynthetic LH1-RC in complex with its electron donor HiPIP. Nat. Commun. *12*, 1104. https://doi.org/10.1038/s41467-021-21397-9.
51. Ninković, D.B., Vojislavljević-Vasilev, D.Z., Medaković, V.B., Hall, M.B., Brothers, E.N., and Zarić, S.D. (2016). Aliphatic-aromatic stacking interactions in cyclohexane-benzene are stronger than aromatic-aromatic interaction in the benzene dimer. Phys. Chem. Chem. Phys. *18*, 25791–25795. https://doi.org/10.1039/c6cp03734h.
52. Zivanov, J., Nakane, T., Forsberg, B.O., Kimanius, D., Hagen, W.J., Lindahl, E., and Scheres, S.H. (2018). New tools for automated high-resolution cryo-EM structure determination in RELION-3. Elife *7*, e42166. https://doi.org/10.7554/eLife.42166.
53. Zivanov, J., Nakane, T., and Scheres, S.H.W. (2020). Estimation of high-order aberrations and anisotropic magnification from cryo-EM data sets in RELION-3.1. IUCrJ *7*, 253–267. https://doi.org/10.1107/S2052252520000081.
54. Zheng, S.Q., Palovcak, E., Armache, J.P., Verba, K.A., Cheng, Y., and Agard, D.A. (2017). MotionCor2: anisotropic correction of beam-induced motion for improved cryo-electron microscopy. Nat. Methods *14*, 331–332. https://doi.org/10.1038/nmeth.4193.
55. Rohou, A., and Grigorieff, N. (2015). CTFFIND4: fast and accurate defocus estimation from electron micrographs. J. Struct. Biol. *192*, 216–221. https://doi.org/10.1016/j.jsb.2015.08.008.
56. Wagner, T., Merino, F., Stabrin, M., Moriya, T., Antoni, C., Apelbaum, A., Hagel, P., Sitsel, O., Raisch, T., Prumbaum, D., et al. (2019). SPHIRE-crYOLO is a fast and accurate fully automated particle picker for cryo-EM. Commun. Biol. *2*, 218. https://doi.org/10.1038/s42003-019-0437-z.
57. Liebschner, D., Afonine, P.V., Baker, M.L., Bunkóczi, G., Chen, V.B., Croll, T.I., Hintze, B., Hung, L.W., Jain, S., McCoy, A.J., et al. (2019). Macromolecular structure determination using X-rays, neutrons and electrons: recent developments in Phenix. Acta Crystallogr. D Struct. Biol. *75*, 861–877. https://doi.org/10.1107/S2059798319011471.
58. Casañal, A., Lohkamp, B., and Emsley, P. (2020). Current developments in coot for macromolecular model building of electron cryo-microscopy and crystallographic data. Protein Sci. *29*, 1069–1078. https://doi.org/10.1002/pro.3791.
59. Pettersen, E.F., Goddard, T.D., Huang, C.C., Couch, G.S., Greenblatt, D.M., Meng, E.C., and Ferrin, T.E. (2004). UCSF Chimera–a visualization system for exploratory research and analysis. J. Comput. Chem. *25*, 1605–1612. https://doi.org/10.1002/jcc.20084.
60. Punjani, A., and Fleet, D.J. (2021). 3D variability analysis: resolving continuous flexibility and discrete heterogeneity from single particle cryo-EM. J. Struct. Biol. *213*, 107702. https://doi.org/10.1016/j.jsb.2021.107702.
61. Qian, P., Hunter, C.N., and Bullough, P.A. (2005). The 8.5Å projection structure of the core RC-LH1-PufX dimer of *Rhodobacter sphaeroides*. J. Mol. Biol. *349*, 948–960. https://doi.org/10.1016/j.jmb.2005.04.032.
62. Madeira, F., Pearce, M., Tivey, A.R.N., Basutkar, P., Lee, J., Edbali, O., Madhusoodanan, N., Kolesnikov, A., and Lopez, R. (2022). Search and sequence analysis tools services from EMBL-EBI in 2022. Nucleic Acids Res. *50*, W276–W279. https://doi.org/10.1093/nar/gkac240.
63. Robert, X., and Gouet, P. (2014). Deciphering key features in protein structures with the new ENDscript server. Nucleic Acids Res. *42*, W320–W324. https://doi.org/10.1093/nar/gku316.
64. UniProt Consortium (2021). UniProt: the universal protein knowledgebase in 2021. Nucleic Acids Res. *49*, D480–D489. https://doi.org/10.1093/nar/gkaa1100.
65. Huokko, T., Ni, T., Dykes, G.F., Simpson, D.M., Brownridge, P., Conradi, F.D., Beynon, R.J., Nixon, P.J., Mullineaux, C.W., Zhang, P., and Liu, L.N. (2021). Probing the biogenesis pathway and dynamics of thylakoid membranes. Nat. Commun. *12*, 3475. https://doi.org/10.1038/s41467-021-23680-1.
66. Huang, F., Kong, W.W., Sun, Y., Chen, T., Dykes, G.F., Jiang, Y.L., and Liu, L.N. (2020). Rubisco accumulation factor 1 (Raf1) plays essential roles in mediating Rubisco assembly and carboxysome biogenesis. Proc. Natl. Acad. Sci. USA *117*, 17418–17428. https://doi.org/10.1073/pnas.2007990117.
67. Williams, C.J., Headd, J.J., Moriarty, N.W., Prisant, M.G., Videau, L.L., Deis, L.N., Verma, V., Keedy, D.A., Hintze, B.J., Chen, V.B., et al. (2018). MolProbity: more and better reference data for improved all-atom structure validation. Protein Sci. *27*, 293–315. https://doi.org/10.1002/pro.3330.

Please cite this article in press as: Bracun et al., Cryo-EM structure of a monomeric RC-LH1-PufX supercomplex with high-carotenoid content from *Rhodobacter capsulatus*, Structure (2023), https://doi.org/10.1016/j.str.2023.01.006



## STAR★METHODS

### KEY RESOURCES TABLE

| REAGENT or RESOURCE | SOURCE | IDENTIFIER |
|---|---|---|
| Chemicals, peptides, and recombinant proteins | | |
| DDM (n-dodecyl β-D-maltoside) | Melford | D12000 |
| Protease Inhibitor Cocktail (PIC) | Melford | P50600 |
| Tris | Melford | T60040 |
| HEPES | Melford | H75030 |
| Sucrose | Fisher Scientific | 11487417 |
| Deposited data | | |
| Cryo-EM density map | This paper | EMDB: EMD-15862 |
| Atomic model | This paper | PDB: 8B64 |
| Experimental models: Organisms/strains | | |
| *Rhodobacter capsulatus* strain SB1003 | ATCC | BAA-309 |
| Software and algorithms | | |
| RELION | Zivanov et al.[52] Zivanov et al.[53] | https://relion.readthedocs.io/en/release-3.1/ |
| MotionCor2 | Zheng et al.[54] | https://emcore.ucsf.edu/ucsf-software |
| CTFFIND-4.1 | Rohou et al.[55] | https://grigoriefflab.umassmed.edu/ctffind4 |
| SPHIRE-crYOLO | Wagner et al.[56] | https://cryolo.readthedocs.io/en/stable/ |
| Phenix | Liebschner et al.[57] | https://phenix-online.org/ |
| COOT | Casanal et al.[58] | https://www2.mrc-lmb.cam.ac.uk/personal/pemsley/coot/ |
| UCSF Chimera | Pettersen et al.[59] | https://www.cgl.ucsf.edu/chimera/ |
| cryoSPARC | Punjani et al.[60] | https://cryosparc.com/ |
| Other | | |
| 300 mesh carbon-support grids | Quantifoil | R1.2/1.3 |
| Vivaspin 6 centrifugal filter unit – 50,000 MWCO | Cytiva | 28932318 |

### RESOURCE AVAILABILITY

#### Lead contact

Further information and requests for resources should be directed to and will be fulfilled by the lead contact, Lu-Ning Liu (luning.liu@liverpool.ac.uk).

#### Materials availability

This study did not generate new unique reagents.

#### Data and code availability

- The cryo-EM density map has been deposited in the Electron Microscopy DataBank (EMDB, www.ebi.ac.uk/pdbe/emdb/) with the accession code EMD-15862, and the atomic coordinates have been deposited in the PDB, www.rcsb.org) with the accession code 8B64. They are publicly available as of the date of publication. Accession numbers are listed in the key resources table.
- This paper does not report original code.
- Any additional information required to reanalyze the data reported in this paper is available from the lead contact upon request.

Please cite this article in press as: Bracun et al., Cryo-EM structure of a monomeric RC-LH1-PufX supercomplex with high-carotenoid content from *Rhodobacter capsulatus*, Structure (2023), https://doi.org/10.1016/j.str.2023.01.006





## EXPERIMENTAL MODEL AND SUBJECT DETAILS

Wild-type *Rhodobacter* (*Rba.*) *capsulatus* strain SB1003 cultures were grown anaerobically in liquid M22 + medium[61] supplemented with vitamins (0.08 M nicotinic acid, 0.01 M thiamine, 7.3 mM 4-aminobenzoic acid, 0.4 mM d-biotin) and 0.1% casamino acids, in tightly closed flasks filled to the top with medium, under 1120 lumen light and in 29°C with 150 rpm shaking. The cultures were left to grow for 7-14 days before protein purification.

## METHOD DETAILS

### Protein purification

The purification of RC–LH1 was carried out following the previous protocol.[19] The WT *Rba. capsulatus* cells were collected by centrifugation at 5,000 ×*g* for 10 min, washed twice with Tris–HCl (pH 8.0) and resuspended in working buffer (20 mM HEPES, pH 8.0). The cell breakage was done by passing the cell suspension through a French press three times at 16,000 p.s.i. Cell debris was pelleted by centrifuging the cell lysate at 20,000 ×*g* for 30 min. The cell membranes were collected by centrifuging the resulting supernatant at 125,000 ×*g* for 90 min. Pelleted membranes were solubilized by incubation in 3% (w/v) DDM (n-dodecyl β-D-maltoside) for 1 h in cold and dark. Unsolubilized materials were then removed by centrifugation (21,000 ×*g*, 30 min, 4°C). Supernatant containing solubilized cell membranes was applied onto the 10–30% (w/v) continuous sucrose gradients made with working buffer and 0.01% (w/v) DDM. Gradients were centrifuged at 230,000 ×*g* for 19 h. The heaviest red/brown pigmented band, representing the RC–LH1 complex, was collected. The buffer containing sucrose was exchanged to working buffer containing 0.01% (w/v) DDM and proteins were simultaneously concentrated using Vivaspin 6 50,000 MWCO column. The purity of the RC−LH1 complex was characterized by SDS-polyacrylamide gel electrophoresis (SDS-PAGE, Figure S1D). A full scan gel image was uploaded to Mendeley and is available as of the date of publication.

### Absorption spectra

Purified RC–LH1–PufX complexes were collected from sucrose gradients and absorbance was measured from 300 to 900 nm at 1-nm intervals using a Libra S22 spectrophotometer (Biochrom, United Kingdom).

### Bioinformatic analysis

Protein sequence alignment was performed using Clustal Omega (EMBL-EBI)[62] and was presented using ESPript 3.0.[63] Phylogenetic tree (Figure S7A) was built using the Uniprot Align tool[64] for the PufX sequences.

### Transmission electron microscopy

The WT *Rba. capsulatus* cells were characterized using thin-section electron microscopy.[65,66] Cells were pelleted by centrifugation (6,000 g, 10 min) and processed for thin section using a Pelco BioWave Pro laboratory microwave system. The cells were first fixed with 0.1 M sodium cacodylate buffer (pH 7.2) supplemented with 2% glutaraldehyde using two steps of 100W for 1 min each (P1). Samples were then embedded in 4% agarose, followed by staining with 2% osmium tetroxide and 3% potassium ferrocyanide using three steps of 100W for 20 s each (P2). The reduced osmium stain was then set in a 1% thiocarbohydrazide solution for 10 min. The second osmium stain was applied using P2 with 2% osmium tetroxide. The sample was made electron dense by incubation with 2% uranyl acetate at 4°C overnight. Dehydration was operated with a series of increasing alcohol concentrations (30–100%) before cells were embedded in medium resin. Thin sections of 70 nm were cut with a diamond knife, followed by a post-stain with 3% lead citrate. Images were recorded on an FEI 120 kV Tecnai G2 Spirit BioTWIN transmission electron microscope (FEI, United States) equipped with a Gatan Rio 16 camera and the DigitalMicrograph software (Gatan, United States).

### Cryo-EM data collection

Three microliters of diluted (1:100) protein solution were applied to the glow-discharged copper grids (Quantifoil R1.2/1.3 Cu, 300 mesh) with a thin carbon-supported film. Grids were plunge-frozen in liquid ethane by Vitrobot Mark IV (Thermo Fisher Scientific). Parameters for plunge freezing were set as follows: blotting time 3 s, waiting time 15 s, blotting force −10, humidity 100%, chamber temperature 4°C. The data were collected on a Titan Krios electron microscope (FEI) using 300 kV electron acceleration and a K3 direct electron detector (Gatan, United States) in counting mode. A total of 6,028 movies were recorded at a nominal magnification of 1,050,00× and a pixel size of 0.8285 Å. The dose rate was 1.05 $e^-$ per $Å^2$ per frame. Defocus ranged from 0.8 to 2.0 μm.

### Data processing

Collected movies were imported into RELION 3.1[52,53] and motion-corrected using MotionCor2.[54] CTF parameters were determined by CTFFIND-4.1.[55] A total of 935,709 particles were picked automatically using SPHIRE-crYOLO[56] with input box sizes of 300 × 300 px. Particles were then extracted in RELION 3.1 and subjected to reference-free 2D classification. After each classification step, the particles that were categorized into poorly defined classes were rejected and only the particles sorted into well-defined classes were selected and processed further. A 3D initial model was calculated in RELION 3.1 based on chosen particles and used as a reference for subsequent 3D classifications of selected particles. Once a well-defined 3D class was obtained, it was refined into a high-resolution electron potential map. The final selected particle number was 181,054. The map then went through several iterations of CTF

parameter refinement, particle polishing and 3D auto-refinement before it was corrected for the modulation transfer function (MTF) of the Gatan K3 summit camera and sharpened by RELION 3.1. The final global map resolution was estimated to be 2.5890 Å on the basis of the Fourier Shell Correlation (FSC) = 0.143 criterion. Local map resolution was calculated by RELION 3.1.

### Modeling and refinement

The atomic model was built using the *Rba. veldkampii* structure (PDB ID: 7DDQ) as a reference starting model.[19] It was fit into the experimentally obtained cryo-EM density map as a rigid body using UCSF Chimera.[59] The sequences were then mutated into those of *Rba. capsulatus* and the resulting model was adjusted manually using COOT.[58] The final model was refined by Phenix 1.18.2,[57] and the stereochemistry was assessed by MolProbity.[67] Most relevant cryo-EM data collection and model validation statistics are summarized in Table S1. All amino acid sequences making up the model are listed in Figure S13. Images were generated and analyzed by UCSF Chimera.[59] 3D variability analysis was performed by using cryoSPARC v4.1.[60] The number of modes to solve was set to 3 and simple output mode was exploited with the number of frames set to 20. B-factors were displayed by UCSF Chimera.

## QUANTIFICATION AND STATISTICAL ANALYSIS

Cryo-EM data collection and refinement statistics are shown in Table S1. 3D classifications of the cryo-EM images were performed in RELION 3.1.[52,53] The final global map resolution was estimated by using the FSC 0.143 criterion. Local map resolution was calculated by RELION 3.1. 3D variability analysis shown in Figure 4 was performed by using cryoSPARC v4.1.[60]